



Cite this: *Mol. Syst. Des. Eng.*, 2020, 5, 1131

Automated determination of *n*-cyanobiphenyl and *n*-cyanobiphenyl binary mixtures elastic constants in the nematic phase from molecular simulation†

Jiale Shi,  ‡ Hythem Sidky‡ and Jonathan K. Whitmer  *

New applications of liquid crystalline materials have increased the need for precise engineering of elastic properties. Recently, Sidky *et al.* [H. Sidky, J. J. de Pablo, and J. K. Whitmer *Phys. Rev. Lett.*, 2018, **120**, 107801] presented methods by which the elastic coefficients of molecular models with atomistic detail can be accurately calculated, demonstrating the result for the ubiquitous mesogen 5CB. However, it is beneficial to future applications to demonstrate how the process may be refined into a precise tool for engineering functional materials. In this work, these techniques are applied to the homologous series of *n*CB materials and their binary mixtures, focusing on the standard bend, twist, and splay deformations, using an automated process. Our results show exceptional agreement with published experimental measurements for the *n*CBs and present a path forward to computational molecular engineering of liquid crystal elasticity for novel molecules and mixtures.

Received 24th May 2019,
Accepted 29th May 2020

DOI: 10.1039/c9me00065h

rsc.li/molecular-engineering

Design, System, Application

Liquid crystalline materials are widely used in industry, and continue to find new uses in technology in custom switchable materials which make use of the molecules' unique optical and geometric properties. Central to each of these applications are the elastic moduli which define the tendency of a liquid crystalline material to resist orientational deformations brought on by surface interactions, electric and magnetic fields, or coupling to mechanical stresses. Here we build on recent results examining the elastic constants of 5CB and extend it to *n*CB molecules using an efficient, automated formalism. This work opens the door to computational investigations of elastic moduli as a tool for computational molecular engineering targeting bespoke elastic properties in pure nematic phases and mixtures.

Introduction

Liquid crystals (LC) are a class of fluids which exhibit long-range orientational ordering and a resistance to spontaneous deformation.¹ While traditionally used in display technologies,² advances in both our understanding of elasticity and material fabrication have opened up many new and interesting applications where the unique properties of LCs can be exploited. Chemoresponsive LCs have been designed to respond to targeted chemical species, which can be quantified through polarized optical microscopy.³ LC elastomeric materials can function as elements in soft robots and sensors.⁴ Topological defects and inclusion formation in LCs have also been used as templates for molecular self-assembly.⁵ Many of these novel applications rely on the

interplay between external, boundary and elastic restoring forces, which is dictated by both the absolute magnitudes and ratios of the elastic constants.

Advances in atomistic simulations have made it possible to gain an unprecedented level of detail into the molecular underpinnings of liquid crystalline behavior which can be rigorously verified against experiment.^{6,7} By understanding the role of molecular features such as conformational flexibility and charge distribution, new LCs can be engineered *in silico* to have highly specific thermophysical properties necessary for biosensing, templating, and other emerging technologies. Until recently,⁸ it was not possible to economically predict the elastic properties of molecular LCs and thus made it extremely difficult to engineer novel LCs for these applications.

The work of Sidky, *et al.*⁸ was a crucial first step in this process, as there it was demonstrated how molecular simulations may be used as a tool to predict the bulk elastic moduli of the molecular liquid crystal models, focusing on the ubiquitous 4-pentyl-4'-cyanobiphenyl, more commonly known as 5CB. There, it was also shown that the saddle-splay elastic constant k_{24} , difficult to obtain in experiments, could

Department of Chemical and Biomolecular Engineering, University of Notre Dame, Notre Dame, IN 46556, France. E-mail: jwhitme1@nd.edu

† Example scripts and information necessary to run the examples contained in this article are posted at https://github.com/shijiale0609/atomistic_elastics.

‡ These authors contributed equally to this work.

be directly measured, and this revealed the underlying positive definite nature of the mode in contradiction to recent experimental suggestions based on indirect observation.^{9–13} The stability of 5CB and its homologues, in addition to their achromic appearance and strong positive dielectric anisotropy, has made them widely used in research^{14,15} and industrial applications.^{1,2} Importantly, their elastic properties have been well-characterized through experiment.^{16–19} Molecular models have also been parameterized to reproduce basic thermodynamic properties such as density, orientational order, and phase transitions.^{20–23}

The focus of this work is on automating the process of determining elastic constants, building on the methodology proposed in ref. 8 to the homologous series of *n*-cyanobiphenyls (*n*CBs) 6CB, 7CB, and 8CB as well as their mixtures. The mesogens in this series are illustrated in Fig. 1. We seek to predict the splay, twist, and bend elastic moduli of *n*CB nematogens through an automated version of the prior algorithms⁸ in order to test the limits and robustness of our methods. This represents a step towards an ultimate goal of computationally-guided LC engineering, and extends the characterization of the elastic properties of existing LC forcefields. We restrict ourselves to the three bulk elastic constants because they are directly measurable in experiment and their behavior is generally well-understood. Although there are minimal structural differences between this series of molecules, the extended alkyl chain has a strong effect on ordering, which gives rise to the “odd–even” effect as the homologous series is ascended.^{16,17,20,24} Though the number *n* is arbitrary, for *n* < 5 nematic phases are not observed, while for *n* > 7, the LC will also admit a smectic phase.

In practical applications, liquid crystal devices tend to utilize mixtures of liquid crystal molecules. Liquid crystals mixtures can be formulated to have a broad nematic phase range, elastic response and dielectric anisotropies which are distinct compared to the components. Elasticity, in particular, is important in determining equilibrium morphologies and material responses. Despite this importance, limited knowledge exists about the connections between microscopic

composition and macroscopic elastic response in liquid crystal blends. Therefore, in this work, we use a representative binary mixture with mole fractions $x_{5CB} = 0.5$ and $x_{8CB} = 0.5$ to explore the splay, twist, and bend moduli of mixtures. We explore the connections between microscopic composition and macroscopic elastic response of liquid crystal blends. This further extends the robustness of our methods.

Methods

The computational methods used here follow ref. 8 closely. For completeness, we will provide a brief summary and highlight the differences. The linear-order elastic free energy density of a uniaxial nematic, absent of any molecular polarity or chirality, may be represented in the Frank–Oseen form.²⁵

$$f = \frac{1}{2}k_{11}(\nabla \times \hat{n})^2 + \frac{1}{2}k_{22}(\hat{n} \times \nabla \times \hat{n})^2 + \frac{1}{2}k_{33}(\hat{n} \times \nabla \times \hat{n})^2 + \frac{1}{2}(k_{22} + k_{24})[\text{Tr}(\nabla \hat{n})^2 - (\nabla \times \hat{n})^2] \quad (1)$$

This expression contains the most commonly used elastic terms: splay (k_{11}), twist (k_{22}) and bend (k_{33}). The additional term, referred to as ‘saddle-splay’, depends on k_{24} and penalizes bidirectional deformations. While the prior work demonstrated this can be measured, the process requires many more molecules to set up the appropriate anchoring and boundary conditions for the problem, and is thus significantly slower. Notably, no measurements of k_{24} exist for *n*CB molecules other than 5CB, limiting available data for validation. We thus focus here on the standard modes of deformation for which data can be readily obtained.

The *n*CB molecules are represented using the united atom forcefield parameterized by Tiberio *et al.*²⁰ After preparing an initial configuration for each molecule type, the process of obtaining elastic constant estimates is entirely automated. Each pure cyanobiphenyl system contains 400 molecules, and is initially prepared by running 100 nanosecond NPT simulations at 1 bar in Gromacs 5.1.3.²⁶ For binary mixtures, the system contains 200 cyanobiphenyl A and 200 cyanobiphenyl B. The temperatures examined are between T_{NI} and $T_{NI} - 20$ K. The transition temperature is independently determined by performing an initial simulation sweep centered on the values reported in ref. 20, and determining when the equilibrium value of the nematic order parameter *S* exceeds 0.1; the measured T_{NI} correspond to those reported in the previous paper. The equilibration time is considerably less than the 400 ns used for 5CB in our previous work, though a reasonable length is necessary to allow for elastic constant prediction at this scale. A Langevin thermostat and Parrinello–Rahman barostat with $\tau_p = 5$ picoseconds are used with a time step of 2 fs for all simulations.

In accordance with ref. 8, the average volume at the each temperature is obtained in the initial round of simulations, and configurations with this volume are automatically drawn from the completed NPT trajectories and used to initiate a second round of NVT simulations with edge restrictions



Fig. 1 The nematic liquid crystal 5CB is related to many other common mesogens, including the homologous series generated by extending the alkyl tail. In this work, we directly measure the elastic constants of 6CB, 7CB, and 8CB from molecular simulation.

applied using a harmonic restraint having modulus $k = 10^5$ kJ mol⁻¹ which serves to align the molecules along the \hat{z} axis. For these simulations we utilize the same timestep as in the constant-pressure case. Four uncorrelated instances are generated at each simulated temperature to function as independent walkers during the elastic measurement, and enhance the convergence of the free energy measurement. The number of independent walkers is known from prior experience to provide sufficient coverage of local free energy landscape, though this number can be tuned to a particular application based on the computational resources available. The simulations at this step were carried out for 400 ns, considerably less than the 1 timescale of the previous study.⁸ We arrived at this number through experimentation, but feel that it is entirely appropriate for most calamitic-type nematogens. Importantly, this step may be trivially parallelized to increase the speed of convergence to the underlying free energy landscape and improve the accuracy of the calculations.

The final step involves estimating the elastic constants from a biased simulation. With edge restrictions in place which align the molecules along the \hat{z} axis, a deformation ξ is applied in the central region according to the elastic mode desired. We take ξ to be $\partial n_x / \partial x$ for splay, $\partial n_y / \partial x$ for twist, and $\partial n_z / \partial z$ for bend. Parabolic free energy profiles obtained *via* the adaptive biasing force method^{27,28} (ABF) as implemented in SSAGES 0.6 (ref. 29) are used to extract the final elastic constant as $f = \frac{1}{2} \gamma k_{ii} \xi^2$ where γ is a geometric factor accounting for the finite restriction and deformation regions.³⁰ To assist readers in reproducing our results, we have posted relevant scripts and Gromacs and SSAGES runfiles in a free online repository located at https://github.com/shijiale0609/atomistic_elastics.

Results and discussion

While data for n CB molecules is more sparse than that for 5CB, a few measurements are available in the literature. We compare all of our calculations to experimental data from ref. 16 and 19; other measurements such as those reported in ref. 17 were not used due to substantial deviations from other reported measurements.

Fig. 2 shows the elastic constant predictions for 6CB. The computed values are in good agreement with experiment across the reported temperature range. The values for k_{33} in particular, match the experimental data very well. While k_{11} is systematically higher than reported experiments, the computed values fall within the typical range variability of experimental measurements reported for 6CB.¹⁶ Twist elastic constants show a larger positive drift away from experimental data as temperature decreases, but remain significantly smaller than the other moduli, as expected, which results in a negative deviation of k_{ii}/k_{22} . For this measurement, there is minimal noise observed in our data for k_{ii} with decreasing $T - T_{NI}$, and the trendline is reasonably smooth and monotonic.



Fig. 2 Bulk elastic constants for 6CB (circles) obtained from molecular simulation. Experimental data obtained from ref. 16 (squares). All elastic constants show good general agreement, with k_{33} exhibiting the least deviation from experiment and k_{22} showing positive deviation, particularly at low temperatures.

The elastic constants for 7CB are shown in Fig. 3. Close to the phase transition temperature T_{NI} , all k_{ii} are in excellent agreement with experimental data. At lower temperature, k_{11} , k_{22} , k_{33} show a positive deviation. But simulated elastic moduli keep the relationship that $k_{33} > k_{11} > k_{22}$. For this measurement, there is still minimal noise observed in our data for k_{ii} with decreasing $T - T_{NI}$, and the trendline keeps reasonably smooth and monotonic. We note that in this case, a systematic overshoot occurs for all k_{ii} relative to the data of ref. 16, similar to what was observed in ref. 8. When considering the behavior relative to the other mesogens modeled here,

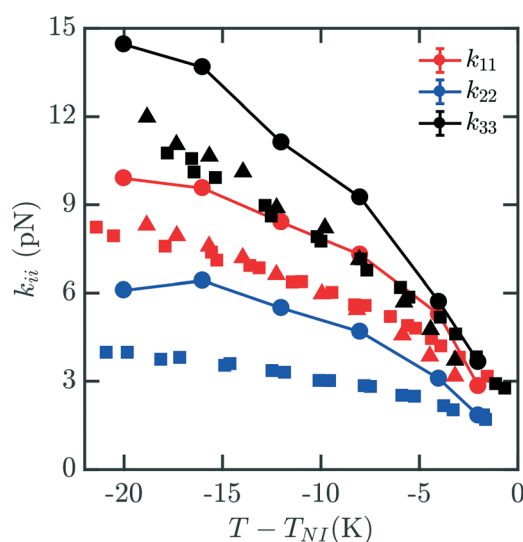


Fig. 3 Bulk elastic constants for 7CB (circles) obtained from molecular simulation. Experimental data obtained from ref. 16 (squares) and 19 (triangles). At low temperature, k_{11} , k_{22} , k_{33} show a positive deviation. But simulated elastic moduli keep the relationship that $k_{33} > k_{11} > k_{22}$.

there is a possibility of an odd-even effect in this overshoot relative to experiments which examined all four homologues.¹⁶

Fig. 4 shows the elastic moduli for 8CB. For $T - T_{NI}$ between -6 K and 0 K (comprising the nematic phase), the simulated elastic constants are in excellent agreement with experimental data. It is well known that 8CB exhibits a smectic A–nematic transition at approximately 7 K below T_{NI} , which results in a divergence of k_{22} and k_{33} .¹⁶ The formation of layers along the nematic axis permits only deformations which are curl-free.³¹ This gives rise to a power-law scaling relation with a critical exponent of $\nu \approx 0.67$.³² However, as the experimental k_{33} and k_{22} begin to diverge near the smectic A–nematic transition, we see that our simulated results do not exhibit the same behavior. It is clear that our measurements are not indicative of the presence of a smectic phase within our simulations.

This apparent discrepancy is due to a number of effects. The first is a strong finite size dependence for the smectic A–nematic transition in this force field model, which has already been reported previously.⁶ Compared to larger systems, those containing fewer than $N = 1000$ mesogens, which is our case, exhibit a considerable discrepancy in smectic ordering.⁶ Similar behaviors were previously observed in combined phase and elastic property simulations of Gay–Berne models.³⁰ The second is that we force the alignment of the 400 mesogens along the \hat{z} axis which may not be the preferred orientation of layers in a fixed-size periodic box. Thirdly, deformations to the mesogens are applied without considering the presence of smectic layering. Finally,



Fig. 4 Bulk elastic constants for 8CB (circles) obtained from molecular simulation. Experimental data obtained from ref. 16 (squares) and 19 (triangles). For $T - T_{NI}$ in the interval $[-6$ K, 0 K] within the nematic phase, the simulated elastic constants are in excellent agreement with experimental data. However, when close to the smectic A–nematic transition we do not observe a divergence in k_{22} and k_{33} commensurate with the formation of a smectic phase. This is due to the suppression and disruption of layered ordering caused by a combination of the free energy sampling process and incommensurate box dimensions in the NVT ensemble suppressing the smectic phase.

simulations are carried out in the NVT ensemble which does not easily permit collective structural relaxation. All of these factors contribute to the suppression and disruption of smectic layering which would manifest in the divergent elasticities absent from our predictions. To properly accommodate and characterize natural smectic layering a semi-isotropic barostat would be necessary, allowing the box dimension ratios to adopt those corresponding to layer separation. The difficulties associated with this within the context of our elastic measurements have been discussed above. In principle, however, the methods we present may be extended to study this intriguing behavior in systems on the order of $N = 3000$ mesogens.⁶ Though we are unable to represent this divergence here, our results across the nematic phase are an excellent match to the experimental results.

Mixtures present a significant challenge for simulations exploring the elasticity of liquid crystals, as they have the potential for spatial inhomogeneity, and must be adequately equilibrated to ensure compositions are uniform and respond as expected to applied stress. The behavior of mixtures of molecules can often exhibit nontrivial dependences on composition which are difficult to predict. Here, we study a representative binary mixture of 5CB and 8CB where each component has a mole fraction of 0.50 ($x_{5CB} = 0.5$ and $x_{8CB} = 0.5$). The resulting mixture has a broadened nematic range relative to 8CB.³³ Elastic measurements for this material were performed using the same protocol as outlined above for pure n CB. Compositions were confirmed to be effectively uniform throughout the simulation box upon equilibration. Fig. 5 shows the computed elastic moduli for this mixture. The raw values of the elastic coefficients are between those of 5CB and 8CB as a function of $T - T_{NI}$, as may be reasonably expected.

To understand how the mixture elasticities relate to the pure component properties, we plot each of the measurements of



Fig. 5 Bulk elastic constants for a mixture with of 5CB and 8CB with mole fractions $x_{5CB} = x_{8CB} = 0.5$.



Fig. 6 Bulk elastic constant k_{11} for the 5CB/8CB binary mixture ($x_{5CB} = x_{8CB} = 0.5$) (black) compared with the calculated k_{11} constants for 5CB⁸ (red) and 8CB (blue). The LC curve (green) is a linear combination of the elastic constants of 5CB and 8CB, weighted by mole fraction.

mixture k_{ii} on the same graph as those for 5CB and 8CB (see Fig. 6–8). The values for k_{11} and k_{22} clearly intercalate the representative nCB values, while, as the values for k_{33} are similar in 5CB and 8CB, all three values are closely bunched. On examination, it appears like our measured values for the mixture are a simple linear combination of the bounding nCB values. To see if this is the case, we plot the linear combinations of the elastic constants (green lines) of the compositions alongside the measurements (black lines) in Fig. 6–8 as a function of $T - T_{NI}$. Quite surprisingly, these two curves lie almost on top of each other, despite all of the potential for nonlinearities in these mixing rules, not the least of which is related to the differences in T_{NI} for the three



Fig. 7 Predicted bulk twist elastic k_{22} constants for 5CB/8CB binary mixture. The curves are defined analogously to Fig. 6.



Fig. 8 Predicted bulk bend elastic k_{33} constants for 5CB/8CB binary mixture. The curves are defined analogously to Fig. 6.

systems. Interestingly, exactly this sort of linear dependence was found in lattice Lebwohl–Lasher mixtures in our prior work.³⁴ This likely means that linear mixing rules can be expected for binary mixtures of chemically similar compounds. Such a linearity likely does not extend to more complex mixtures, or dissimilar chemical compositions. Still, development of simple correlations for liquid crystalline materials could be of great utility for engineering specific elastic properties in to LC-based materials and devices, and molecular simulations will be extremely useful to inform them.

Conclusion

In this work we have estimated the elastic constants of the cyanobiphenyls 6CB, 7CB, 8CB and binary mixtures ($x_{5CB} = 0.5$, $x_{8CB} = 0.5$) from biased molecular simulation using an entirely automated procedure. We show that the simulated elastic moduli of the cyanobiphenyls are generally in good agreement with reported experimental values. We find that the simulated elastic moduli of binary mixtures generally follow a linear combination of the compositions with reduced temperature. Difficulties arise in generating meaningful uncertainties and dealing with the onset of the smectic phase for 8CB. Both improving the prediction accuracy and applying this methodology on a large scale are only possible if the cost of elasticity measurements is substantially reduced. Currently, up to 4 μ s of total simulation runtime is required to generate a estimate of a single elastic mode at a single temperature.

Developing newer or better optimized sampling algorithms may significantly reduce this time and open the door to *in silico* liquid crystal engineering. This would necessitate some means of attenuating early-time noise present in elastic measurements, and perhaps a simplification of the order-parameter calculation which is computationally expensive and involves third-order tensor

algebra. As presented, the methodology developed is capable of producing accurate elastic constants and merits further study to elucidate the precise limit of efficiency while retaining measurement fidelity. Further, a crucial next step involves moving beyond cyanobiphenyls and examine atomistic models of the myriad liquid crystal phases, from molecules of historical interest, such as PAA and MBBA^{35,36} to more exotic bent-core molecules and models exhibiting chiral³⁷ or twist-bend phases.³⁸ Improving the breadth, speed, and accuracy of these techniques will enable their use in computational screening of new mesogenic compounds.

Conflicts of interest

There are no conflicts to declare.

Acknowledgements

HS acknowledges support from the National Science Foundation Graduate Research Fellowship Program (NSF-GRFP). JS and JKW acknowledge the support of MICCoM, the Midwest Center for Computational Materials, as part of the Computational Materials Sciences Program funded by the U.S. Department of Energy, Office of Science, Basic Energy Sciences, Materials Sciences and Engineering Division, for the development of algorithms and codes used within this work. JS, HS and JKW additionally acknowledge computational resources at the Notre Dame Center for Research Computing (CRC).

References

- 1 M. Kleman and O. D. Lavrentovich, *Soft Matter Physics: An Introduction*, Springer-Verlag, New York, 1st edn, 2003.
- 2 G. W. Gray and S. M. Kelly, *J. Mater. Chem.*, 1999, **9**, 2037–2050.
- 3 T. Szilvási, L. T. Roling, H. Yu, P. Rai, S. Choi, R. J. Twieg, M. Mavrikakis and N. L. Abbott, *Chem. Mater.*, 2017, **29**, 3563–3571.
- 4 G. Babakhanova, T. Turiv, Y. Guo, M. Hendriks, Q.-H. Wei, A. P. H. J. Schenning, D. J. Broer and O. D. Lavrentovich, *Nat. Commun.*, 2018, **9**, 456.
- 5 X. Wang, D. S. Miller, E. Bukusoglu, J. J. de Pablo and N. L. Abbott, *Nat. Mater.*, 2015, **15**, 106–112.
- 6 M. F. Palermo, A. Pizzirusso, L. Muccioli and C. Zannoni, *J. Chem. Phys.*, 2013, **138**, 204901.
- 7 H. Ramezani-Dakhel, M. Sadati, M. Rahimi, A. Ramirez-Hernandez, B. Roux and J. J. de Pablo, *J. Chem. Theory Comput.*, 2017, **13**, 237–244.
- 8 H. Sidky, J. J. de Pablo and J. K. Whitmer, *Phys. Rev. Lett.*, 2018, **120**, 107801.
- 9 D. W. Allender, G. P. Crawford and J. W. Doane, *Phys. Rev. Lett.*, 1991, **67**, 1442–1445.
- 10 A. Sparavigna, O. D. Lavrentovich and A. Strigazzi, *Phys. Rev. E: Stat. Phys., Plasmas, Fluids, Relat. Interdiscip. Top.*, 1994, **49**, 1344–1352.
- 11 R. D. Polak, G. P. Crawford, B. C. Kostival, J. W. Doane and S. Žumer, *Phys. Rev. E: Stat. Phys., Plasmas, Fluids, Relat. Interdiscip. Top.*, 1994, **49**, R978–R981.
- 12 E. Pairam, J. Vallamkondu, V. Koning, B. C. van Zuiden, P. W. Ellis, M. A. Bates, V. Vitelli and A. Fernandez-Nieves, *Proc. Natl. Acad. Sci. U. S. A.*, 2013, **110**, 9295–9300.
- 13 Z. S. Davidson, L. Kang, J. Jeong, T. Still, P. J. Collings, T. C. Lubensky and A. G. Yodh, *Phys. Rev. E: Stat., Nonlinear, Soft Matter Phys.*, 2015, **91**, 050501.
- 14 X. Wang, D. S. Miller, E. Bukusoglu, J. J. de Pablo and N. L. Abbott, *Nat. Mater.*, 2016, **15**, 106–112.
- 15 H. Eimura, D. S. Miller, X. Wang, N. L. Abbott and T. Kato, *Chem. Mater.*, 2016, **28**, 1170–1178.
- 16 N. V. Madhusudana and R. Pratibha, *Mol. Cryst. Liq. Cryst.*, 1982, **89**, 249–257.
- 17 H. Hakemi, E. F. Jagodzinski and D. B. DuPre, *J. Chem. Phys.*, 1983, **78**, 1513.
- 18 G.-P. Chen, H. Takezoe and A. Fukuda, *Liq. Cryst.*, 1989, **5**, 341–347.
- 19 P. Chatopadhyay and S. K. Roy, *Mol. Cryst. Liq. Cryst. Sci. Technol., Sect. A*, 1994, **257**, 89–98.
- 20 G. Tiberio, L. Muccioli, R. Berardi and C. Zannoni, *ChemPhysChem*, 2009, **10**, 125–136.
- 21 N. J. Boyd and M. R. Wilson, *Phys. Chem. Chem. Phys.*, 2015, **17**, 24851–24865.
- 22 I. Cacelli, L. De Gaetani, G. Prampolini and A. Tani, *J. Phys. Chem. B*, 2007, **111**, 2130–2137.
- 23 I. Cacelli, C. F. Lami and G. Prampolini, *J. Comput. Chem.*, 2009, **30**, 366–378.
- 24 G. W. Gray and K. J. Harrison, *Symp. Faraday Soc.*, 1971, **5**, 54–67.
- 25 I. W. Stewart, *The static and dynamic continuum theory of liquid crystals: a mathematical introduction*, Taylor & Francis, London, 2004.
- 26 M. J. Abraham, T. Murtola, R. Schulz, S. Páll, J. C. Smith, B. Hess and E. Lindahl, *SoftwareX*, 2015, **12**, 19.
- 27 E. Darve, D. Rodriguez-Gomez and A. Pohorille, *J. Chem. Phys.*, 2008, **128**, 144120.
- 28 J. Comer, J. C. Gumbart, J. Hénin, T. Lelièvre, A. Pohorille and C. Chipot, *J. Phys. Chem. B*, 2014, **119**, 1129–1151.
- 29 H. Sidky, Y. J. Colón, J. Helfferich, B. J. Sikora, C. Bezik, W. Chu, F. Giberti, A. Z. Guo, X. Jiang and J. Lequieu, *et al.*, *J. Chem. Phys.*, 2018, **148**, 044104.
- 30 A. A. Joshi, J. K. Whitmer, O. Guzmán, N. L. Abbott and J. J. de Pablo, *Soft Matter*, 2014, **10**, 882–893.
- 31 P. de Gennes, *Solid State Commun.*, 1972, **10**, 753–756.
- 32 H. Hakemi, *Liq. Cryst.*, 1989, **5**, 327–339.
- 33 S. Fujimura, Y. Yamamura, M. Hishida, S. Nagatomo and K. Saito, *Liq. Cryst.*, 2014, **41**, 927–932.
- 34 H. Sidky and J. K. Whitmer, *Soft Matter*, 2016, **12**, 4489–4498.
- 35 I. Haller, *J. Chem. Phys.*, 1972, **57**, 1400–1405.
- 36 W. H. D. Jeu, W. A. P. Claassen and A. M. J. Spruijt, *Mol. Cryst. Liq. Cryst.*, 1976, **37**, 269–280.
- 37 I. Dierking, *Symmetry*, 2014, **6**, 444–472.
- 38 D. Chen, J. H. Porada, J. B. Hooper, A. Klittnick, Y. Shen, M. R. Tuchband, E. Korblova, D. Bedrov, D. M. Walba, M. A. Glaser, J. E. MacLennan and N. A. Clark, *Proc. Natl. Acad. Sci. U. S. A.*, 2013, **10**, 15931.